Impact properties of an end of life tires' rubber. Numerical validation considering large strain and strain rate conditions

Joaquín González-Vega[1], Germán Castillo-López[2], and Felipe García-Sánchez[3,*]

[1]Departamento de Ingeniería Civil, de Materiales y Fabricación. Escuela de Ingenierías Industriales. Universidad de Málaga. Spain
[1]ORCID: 0000-0002-9999-0379
[2] ORCID: 0000-0002-8898-3376
[4]ORCID: 0000-0001-9314-8183
[*]Corresponding author: fgsanchez@uma.es

February 19, 2024

Highlights:

- Properties of a revulcanized rubber are evaluated under impact loads
- The analyzed rubber come from recycled end-of-life tires
- Impact loads under large strain and high strain rates are considered
- The Bergström-Boyce behavior model has been considered to fit the properties of the materials
- Numerical validation is done using two solvers on LS-DYNA software®

Abstract

In a previous work, the experimental viscoelastic properties of a renewed rubber obtained from the recycling of end-of-life tires (ELTs) were presented, [1]. The material was tested in the laboratory by means of impact tests that revealed how the behavior of the rubber depends on the strain rate in such a case. Due to the loading conditions of high strains and high strain rates, the nonlinear viscoelastic Bergtröm-Boyce (BB) model, defined by nine parameters, was selected to fit the behavior of the material.

To obtain the parameters from the results of the impact tests, different optimization methods were used. As many sets of nine parameters were obtained as optimization methods were considered, with notable differences between them in some cases.

The motivation of this work is to know which set of parameters, i.e. which optimization method, is the most appropriate. With this objective, a complete comparative numerical analysis of these sets, forty-eight in total, has been developed by means of simulations performed in LS-DYNA software.

As a result of this analysis, the model that best suits the behavior of the material for the load case studied was chosen. This work completes the first step to reach the final objective of our research, which is to numerically analyze the behavior of systems designed to absorb energy in impact events based on this material.

Keywords: End-of-life tires (ELTs), Rubber numerical analysis, Nonlinear viscoelastic models, Numerical rubber model validation, Bergtröm-Boyce (BB) model.

1 Introduction

End-of-life tires (ELTs from here on) are those tires that have reached the end of their useful life, becoming, since this moment, a big environmental problem. The reason for that environmental problem is its main component: rubber designed to withstand the most extreme conditions. Consequently, this rubber is reduced, after its useful life, to a waste difficult to eliminate.

Currently, the two main ways to manage this problem are: (i) using this waste as fuel due to its high calorific value or (ii) to reuse this material either for a different purpose, as raw material for other products or in any other way.

The numerical analysis of this type of materials is of great interest since, in this way, it is possible to study their applicability to different uses. For this reason, there are numerous recent studies on the matter. Some of them are listed below.

Pan et al. [2] developed a mesoscale model of rubberised concrete with different crumb rubber contents up to 30% to evaluate the dynamic characteristics of the rubberised concrete. The existing experimental data proved the accuracy of the numerical model.

Gao et al. [3] proposed a new form of double layer rubber dam to improve the water-retaining ability of conventional rubber dam. Numerical studies using $FLAC^{2D}$ software were carried out to analyze the behavior of the proposed method. The numerical model was verified by the results from the laboratory model tests and analytical studies in literature.

Dhir et al. [4] have published a study about a novel mesoscale approach for simulating the response of reinforced concrete frames equipped with masonry infill walls and rubber joints under horizontal loads such as those induced by earthquakes.

Yang et al. [5] developed an aircraft tire and grooved runway models according to finite element (FE) simulations. The interaction model for the aircraft tire and grooved runway was developed using the Power Spectrum Density (PSD) and the viscoelastic properties of tread rubber. The FE model was validated for skid resistance by conducting runway field experiments.

Leng et al. [6] presented an experimental and numerical method on stress relaxation and unrecoverable damage characteristics of rubber materials.

Liu et al. [7] carried out a study focused on the heterogeneous deformation and heat build-up of the crack tip region in a rubber fatigue crack growth rate (FCGR) test.

Zhuo et al.[8] made numerical simulations and model tests conducted to study the influence of rubber fraction by volume (RF) on the macro/micro mechanical characteristic of lightweight fill material (LFM) and its engineering applications. The influence of LFM buried depth on the deformation of cut-and-cover tunnel (CCT), earth pressure around CCT, and vertical displacement of backfill sand above CCT were also discussed.

Šulc et al. [9] presented a new proposal for modeling the damping of hard rubbers at large deformations and quasi-harmonic excitation in the low frequency range. A torsion stand was designed and manufactured for rubber testing. According to the results of the experiments, the hyperelastic proportional damping (HPD) model based on the generalized Rivlin hyperelastic material model is sufficiently accurate and, in addition, is easy to implement in a FE code.

Nguyen et al. [10] developed analytical formulations and non-linear numerical models to study the behaviour of natural rubber bearings incorporating U-shaped damper devices under cyclic loadings.

Sheikhi et al [11] evaluated a natural rubber bearing system (NRB) equipped with a damper under lateral loading. U-shaped dampers with shape memory and steel alloy materials were used. The effect of parameters such as shear strain amplitude, the optimal thickness ratio of shaped memory alloy (SMA) to structural steel, NRB shape factor, thickness of SMA dampers, and the effect of lateral loading directions on the performance characteristics of bearing system were investigated. Mooney-Rivlin and Prony models were selected for modeling the rubber material in ANSYS® FE software.

Modheg et al. [12] modeled a visco-hyperelastic damper (VHD) according to steel and rubber test results using high axial damping rubber in VHD under harmonic loading.

With the broader aim of working towards the development of a class of comprehensive hyperelastic models, Anssari et al. [13] utilised a three-parameter strain energy function for application to various types of isotropic rubber-like materials.

In a recent work [1], the authors of the present one analyzed experimentally a new recycled rubber from ELTs produced by the Danish company genan®. The recycled material, thanks to a re-vulcanization process, becomes a renewed rubber. Unfortunately, due to the manufacturing procedure its shape is restricted to small pellets, as it is shown in Figure 1. This limiting aspect causes its use needs the help of a resin acting as binder.

In [1] the material was calibrated, considering the nonlinear viscoelastic Bergström-Boyce (BB) model, by mean of compression impact tests under different impact velocities. Due to its agglomerated typical use,

Figure 1: Appearance of longest pellets manufactured from ELTs by genan®.

the tests were done over pellets in its original presentation and coated with a polyurethane resin. Throughout these tests, the energy dissipation capacity of this material was also evaluated. The nine material properties defining the BB model were computed via several optimization techniques, applied to the experimental records, using MCalibration® software. As it is expectable, each optimization technique gives a different set of material constants capable, in theory, to capture the viscoelastic behavior of the material.

The present work focuses on the numerical analysis of the problem investigating how accurate are really those sets of constants by mean of their implementation in a FE model. With this aim the impact tests are simulated using the LS-DYNA® software according two versions:

- The native approach of LS-DYNA®.
- A modified approach (running under LS-DYNA®) called PolyUMod® specifically designed, among others, for the considered nonlinear viscoelastic model, developed by PolymerFEM®.

The following section, Section 2, presents the two BB model formulations considered in the present work. Section 3 shows the different sets of constants obtained for both BB formulations using MCalibration® software. As the work developed in [1] yielded to sets of material parameters according to only one of the formulations examined here, a new calibration procedure to obtain new parameter sets, coherent with the new formulation, has been done. This section also summarizes a comparative analysis of the different sets of parameters obtained for both approaches. Section 4 is devoted to the numerical analysis. It describes the used model and the obtained results. Three cases of impact velocities are investigated, covering a strain rates range from 133.33 s^{-1} to 400 s^{-1}. Finally, the manuscript ends with concluding remarks in Section 5.

2 Bergström-Boyce model formulations.

Since its publication in 1998, [14], the non linear viscoelastic behavior defined by the Bergstöm-Boyce model has been slightly modified to include more aspects of polymer's behavior, making it more and more generalist, see [15]. This model is based on the eight chains (EC) hyperelastic model published by Arruda and Boyce in 1993 to describe the elastic behavior of rubbers, [16].

In the present work two slightly different approaches are considered for the model. Each one brings us to a different solver running, both, under LS-DYNA® software.

One solver, in fact the native LS-DYNA® solver, is based on the work published in 2009 by Dal and Kaliske, [17]. The other solver, called PolyUmod®, has been developed by PolymerFEM®. In the following sections both approaches are briefly depicted.

2.1 PolyUMod® formulation

Conceptually, BB model is represented by two networks (or branches) acting in parallel (Fig. 2, left). One branch (let's say branch a) contain only hyperelastic information while the other (let's say branch b) capture the non-linear viscoelastic behavior in series with hyperelastic information as well. The hyperelastic behavior of each of these branches must be understood under the eight-chain macromolecular networks concept by Arruda and Boyce, [16].

Due to the parallel arrangement of branches a and b, the deformation gradient acting on the whole model is the same for both branches (Fig. 2, right). For the same reason, the total stress of the model is the sum of elastic stresses of each branch. Mathematically:

$$\mathbf{F} = \mathbf{F}_a = \mathbf{F}_b \tag{1}$$

$$\boldsymbol{\sigma} = \boldsymbol{\sigma}_a + \boldsymbol{\sigma}_b \tag{2}$$

In eq. (1), $\mathbf{F}$ stands for deformation gradient tensor and, in eq. (2), $\boldsymbol{\sigma}$ denotes the Cauchy stress tensor. Note: as usual, boldface has been used for tensors and normal text for scalars.

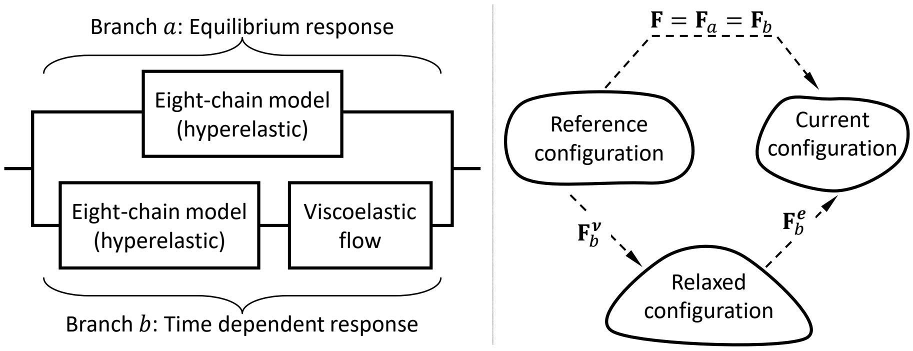

Figure 2: Conceptual representation of Bergström-Boyce model (left) and consequent multiplicative decomposition of deformation (right).

In accordance with the constitutive equation of the eight-chain model, [16], the Cauchy stress tensors for the networks a and b have the following form:

$$\boldsymbol{\sigma} = \frac{\mu}{J\overline{\lambda^*}} \frac{\mathcal{L}^{-1}\left(\overline{\lambda^*}/\lambda^{lock}\right)}{\mathcal{L}^{-1}\left(1/\lambda^{lock}\right)} \operatorname{dev}\left[\mathbf{b}^*\right] + k\left(J-1\right)\mathbf{I} \tag{3}$$

In eq. (3):

- $J = \det(\mathbf{F})$, where $\det(\cdot)$ stands for tensor's determinant.
- **b*** is the distortional (constant volume) part of left Cuchy-Green tensor.
- μ is the initial shear modulus of the material.
- k is the bulk modulus.
- $\overline{\lambda^*} = \left[\operatorname{tr}(\mathbf{b}^*)/3\right]^{1/2}$, being $\operatorname{tr}(\cdot)$ is the trace of the tensor.
- $\mathcal{L}$ is the Lanvegin function: $\mathcal{L}(x) = \coth(x) - 1/x$.
- $\mathbf{I}$ stands, as usual, for the identity matrix.

Of course, the time dependence of the model must be in the viscoelastic branch b. The BB model decomposes its deformation gradient tensor into the product of its elastic (e) and viscoelastic (v) components, as shown in eq. (4).

$$\mathbf{F}_b = \mathbf{F}_b^e\,\mathbf{F}_b^v \tag{4}$$

In order to complete the model, see [15] for further details, it is necessary to consider the spatial velocity gradient of branch b ($\mathbf{L}_b$), related with deformation gradient tensor as is indicated in eq. (5).

$$\mathbf{L}_b = \dot{\mathbf{F}}_b\,\mathbf{F}_b^{-1} \tag{5}$$

Following [15], this tensor is decomposed in elastic and viscous components, eq. (6),

$$\mathbf{L}_b = \mathbf{L}_{be} + \mathbf{D}_{bv} \tag{6}$$

and the viscous component $\mathbf{D}_{bv}$ is expressed as in eq. (7).

$$\mathbf{D}_{bv} = \dot{\gamma}_0 \left(\overline{\lambda_{bv}} - 1 + \xi\right)^C \left[R\left(\frac{\tau}{f_v \tau_{base}} - \hat{\tau}_{cut}\right)\right]^m \frac{\mathrm{dev}(\boldsymbol{\sigma}_B)}{\tau} \tag{7}$$

Where

- $R(x) = (x + |x|)/2$, is the ramp function.
- f_v is a *network interaction factor* to capture the observed behavior for most elastomers having different strain-rate dependence during loading than unloading.
- τ is the effective stress driving the viscous flow defined as $\tau = ||\mathrm{dev}[\sigma_B]||$, being $||\ ||$ the Frobenius norm here and hereinafter.
- $\dot{\gamma}_0$ is a constant introduced for dimensional consistency called reference strain rate.
- $\left(\overline{\lambda_{bv}} - 1 + \xi\right)^C$ is a term introduced by reptational dynamics. This term captures a stretch dependence of the effective viscosity, see [18].
- ξ, C, τ_{base}, $\hat{\tau}_{cut}$ and m; are material constants. In particular, ξ is small positive constant introduced to eliminate a removable singularity in the flow rate in the undeformed state [15].

In summary, the constants set necessary to fully define a BB material following this approach, i.e., to solve the model using the PolyUMod® solver, are the ones shown in table 1.

Table 1: Material constants for PolyUMod® solver, [19].

Mat. param.	Name/Meaning
$\mu\,[MPa]$	Shear modulus of network a
$k\,[MPa]$	Bulk modulus
$\lambda_L\,[-]^*$	Locking stretch
$s\,[-]$	Relative stiffness of network b
$\xi\,[-]$	Strain adjustment factor
$C\,[-]$	Strain exponential
$\tau_{base}\,[MPa]$	Flow resistance
$m\,[-]$	Stress exponential
$\hat{\tau}_{cut}\,[-]$	Normalized cut-off stress for flow

* Note: $[-]$ stands for non-dimensional parameters.

2.2 LS-DYNA® formulation

The native formulation of LS-DYNA® for BB model, based on [17] (of course, founded on the theory of parallel branches), follows the idea that the volumetric part is elastic and governed by the bulk modulus (k) and the deviatoric Kirchhoff stress tensor ($\overline{\boldsymbol{\tau}}$) is the sum of an elastic ($\overline{\boldsymbol{\tau}}_e$) and a viscoelastic part ($\overline{\boldsymbol{\tau}}_v$).

These deviatoric terms, following again the EC model in [16], are, in this case, written as following:

$$\overline{\boldsymbol{\tau}}_e = \frac{G}{3}\frac{3-\lambda_r^2}{1-\lambda_r^2}\left(\overline{\mathbf{b}} - \frac{\mathrm{tr}\left(\overline{\mathbf{b}}\right)}{3}\mathbf{I}\right), \tag{8}$$

$$\overline{\boldsymbol{\tau}}_v = \frac{G_v}{3}\frac{3-\lambda_v^2}{1-\lambda_v^2}\left(\overline{\mathbf{b}}_e - \frac{\mathrm{tr}\left(\overline{\mathbf{b}}_e\right)}{3}\mathbf{I}\right), \tag{9}$$

being

- $\overline{\mathbf{b}} = J^{-2/3}\mathbf{F}\mathbf{F}^T$ with $J = \det(\mathbf{F})$
- $\overline{\mathbf{b}}_e = \mathbf{F}_e\mathbf{F}_e^T$ with $J^{-1/3}\mathbf{F} = \mathbf{F}_e\mathbf{F}_i$, where subindices e and i stands for elastic and inelastic parts, respectively.
- G and G_v are the elastic and viscoelastic shear modulus, respectively.
- $\lambda_r^2 = \mathrm{tr}\left(\overline{\mathbf{b}}\right)/(3N)$ and $\lambda_v^2 = \mathrm{tr}\left(\overline{\mathbf{b}}_e\right)/(3N_v)$, where N and N_v are the numbers of elastic and viscoelastic segments, respectively.

The time evolution is introduced in this approach via the inelastic rate-of-deformation tensor $(\mathbf{D}_i)$ expressed as in eq. (10).

$$\mathbf{D}_i = \dot{\gamma}_0 \left(\lambda_i - 0.999\right)^c \left(\frac{||\overline{\boldsymbol{\tau}}_v||}{\hat{\tau}\sqrt{2}}\right)^m \frac{\overline{\boldsymbol{\tau}}_v}{||\overline{\boldsymbol{\tau}}_v||} \tag{10}$$

Where

- $\dot{\gamma}_0$ is the reference strain rate.
- $\hat{\tau}$ is the reference Kirchhoff stress.
- $\lambda_i = \mathrm{tr}\left(\mathbf{F}_i^T \mathbf{F}_i\right)/3$.
- c and m are, respectively, the inelastic strain and stress exponents.

As it has been stated above, the volumetric part of the model is elastic and governed by the bulk modulus (k). According to that, the pressure (p) is given by:

$$p = \left(J^{-1} - 1\right) k. \tag{11}$$

In consequence, the constants set necessary to solve the BB model according to this formulation are summarized in table 2.

Table 2: Material constants for LS-DYNA® native solver, [20].

Mat. param.	Name/Meaning
$k\,[MPa]$	Elastic bulk modulus
$G\,[MPa]$	Elastic shear modulus
$G_v\,[MPa]$	Viscoelastic shear modulus
$N\,[-]^*$	Elastic segment number
$N_v\,[-]$	Viscoelastic segment number
$C\,[-]$	Inelastic strain exponent
$m\,[-]$	Inelastic stress exponent
$\dot{\gamma}_0\,[1/s]$	Reference strain rate
$\hat{\tau}\,[MPa]$	Reference Kirchhoff stress

* Note: $[-]$ stands for non-dimensional parameters.

3 Material calibrations

Hereinafter, when necessary, the different sets of constants will be denoted by LS-set and PUM-set for LS-DYNA® and PolyUmod® solvers, respectively.

In the previous work, [1], the authors presented the experimental procedure to obtain the PUM-sets via compression impact test over original pellets, i.e., pellets as obtained from the recycled procedure, and over pellet with coating polyurethane resin 8wt%. In the present work, for comparison purposes, the same procedure has been used to obtain LS-sets.

As stated above, software MCalibration®, by PolymerFEM®, has been used to perform the model calibration. The utilized version (6.2.0) offers twelve different ways of calibration by combining three objective functions and four calibration algorithms, see [1] for a complete description of the calibration process. Taking into account that we have two kind of specimens, coated (with polyurethane) and uncoated (in raw form) and two sets of parameters, LS and PUM sets, we have a total of forty-eight combinations. For the sake of completeness, all sets of experimental parameters have been summarized in the Appendix: tables 3, 4, 5 and 6.

Looking those tables, some differences between properties, obtained from different optimization procedures, appear to be very significant. Looking for any conclusion about it, in the following, the results for the used calibration methods will be represented with respect to their averaged values.

Trying to draw any trend regarding the optimization process, all sets of properties have been plotted in normalized way. With this aim, each parameter has been normalized by mean of the averaged values obtained using the four algorithms, for each objective function. Of course, this normalization procedure has not physical meaning, but is able to show, at a glance, how different are the results given for different algorithms.

The normalized parameters, denoted by and asterisk, are sumarized in Figs. 3 - 6. These plots have been grouped by objective function (R^2, MSD and NMAD) and represented vs. the calibration algorithm (GSM, EAM_1, EAM_2 and QAM). See [1] for more information about calibration algorithms and objective functions.

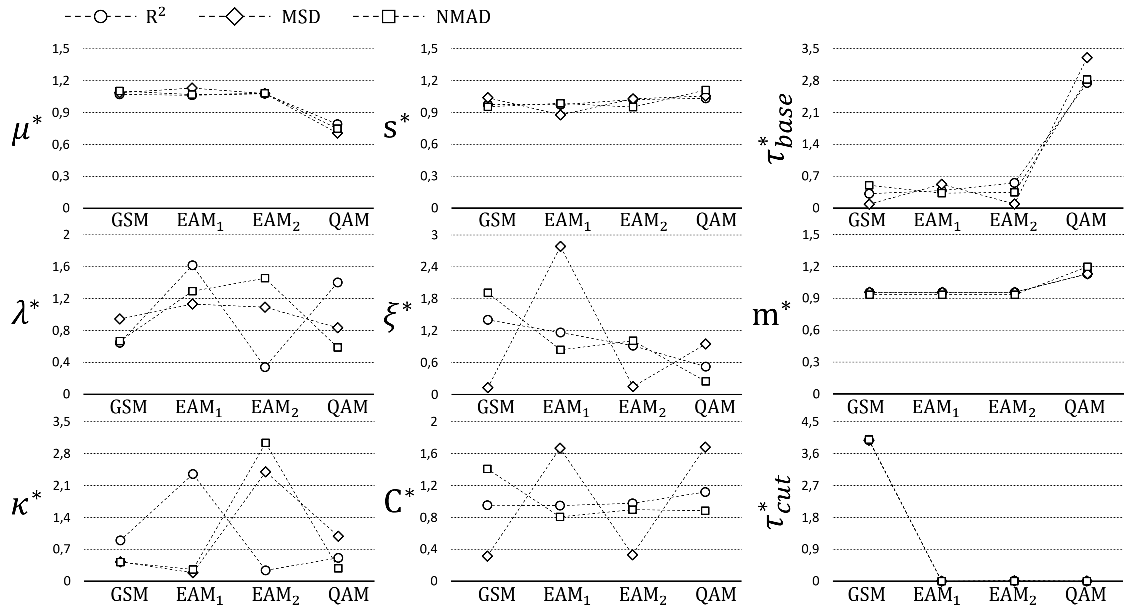

Figure 3: Normalized PUM-set constants obtained for all the considered optimization procedures. Uncoated rubber.

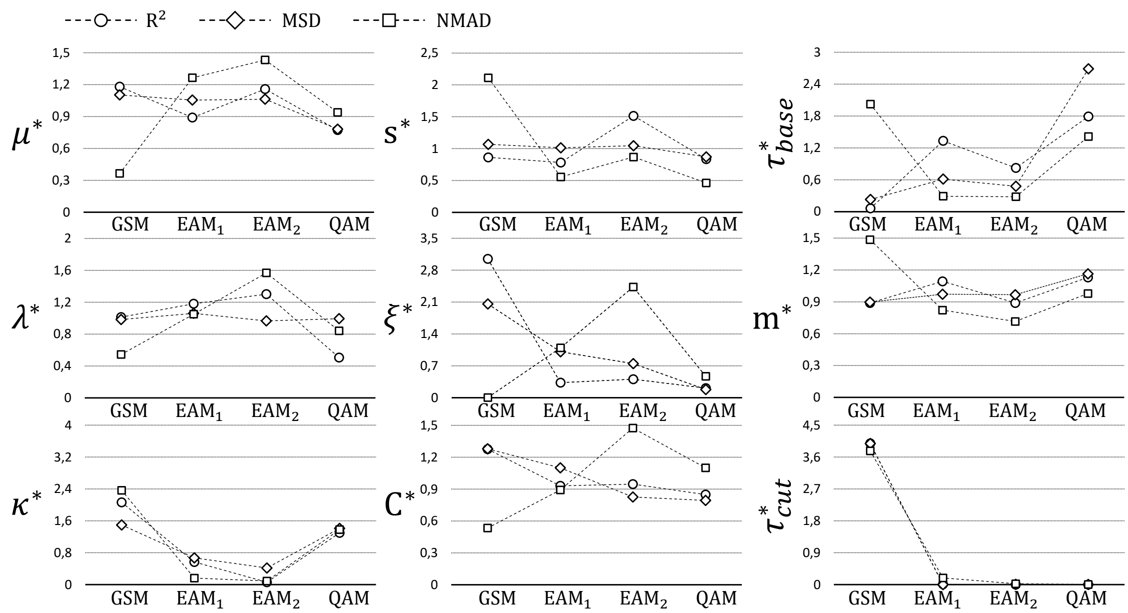

Figure 4: Normalized PUM-set constants obtained for all the considered optimization procedures. Coated rubber.

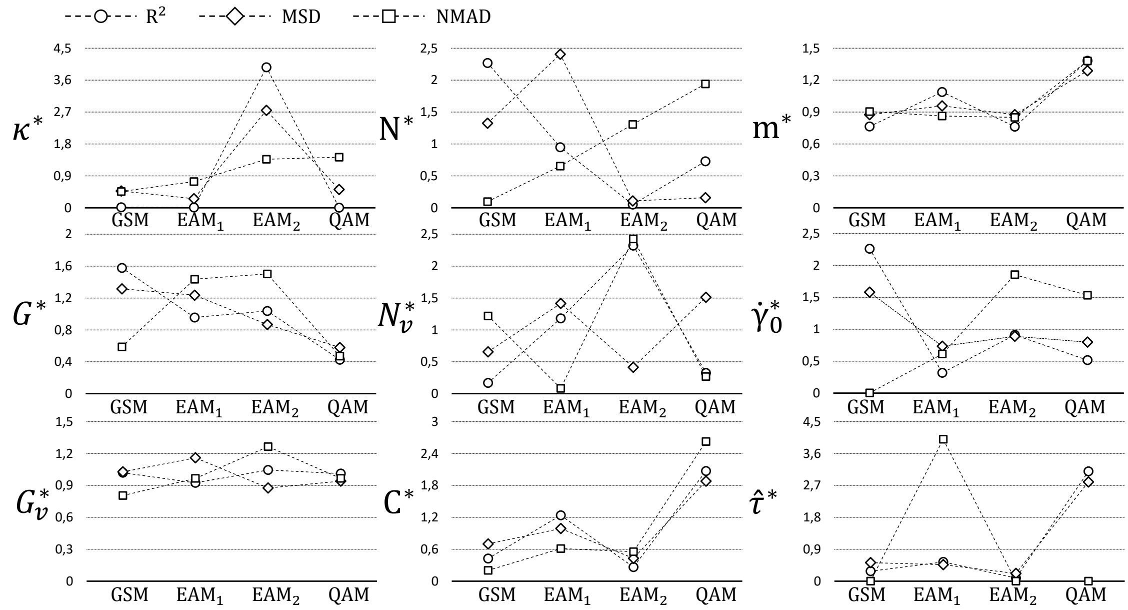

Figure 5: Normalized LS-set constants obtained for all the considered optimization procedures. Uncoated rubber.

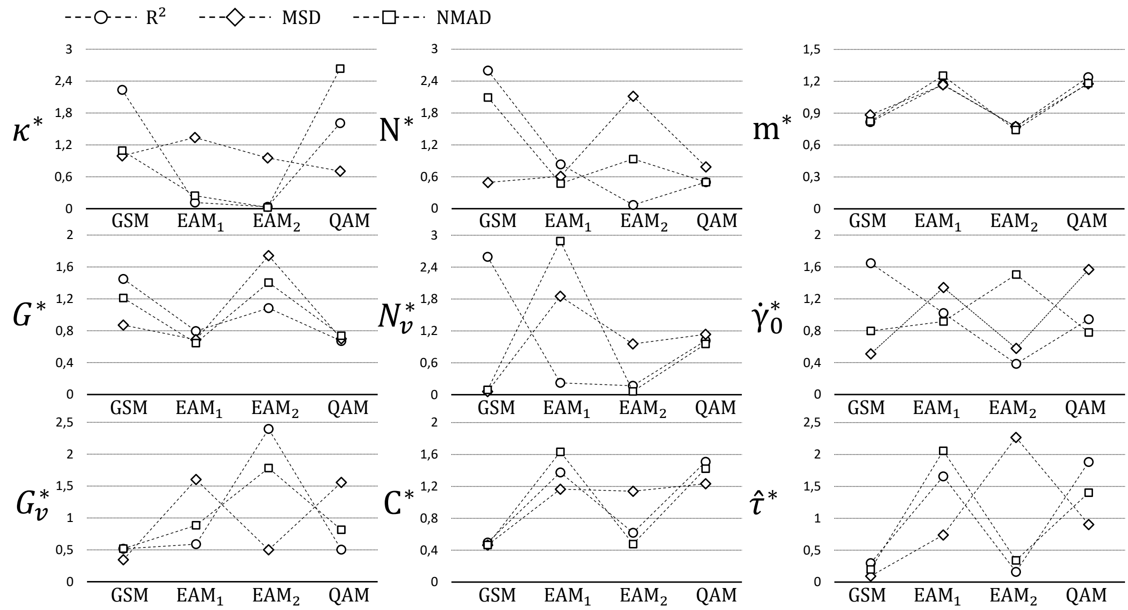

Figure 6: Normalized LS-set constants obtained for all the considered optimization procedures. Coated rubber.

As it can be observed, exceptionally, the value of any of the materials parameters remain quite stable, i.e., its normalized value remain near to one, for example μ^* or m^* in Fig. 3. However, most of the values show big (and random) variations that can reach values 300% or even more: ξ^* in Figs. 3 or 4, κ^* and N_ν^* in Figs. 5 and 6, respectively, among many others. Consequently, it is clear that no pattern can be observed at all. Taking this into account and on the basis of the numerical results that will be shown latter on, the conclusion is that attempting to analyze, individually, each parameter is a mistake. Every group of parameters has to be understood as a whole. So that, two groups of very different parameters can give rise to a very similar viscoelastic behavior, as will be seen in the next section.

4 Numerical study

In this section the numerical results obtained for all material properties summarized in the Appendix are presented.

The compression impact tests in [1] were applied to rubber cylinders by an aluminum-made cylindrical hammer, see Figure 7 left. To record the reaction during the impact, the specimens were placed over a load cell, see Figure 7 right.

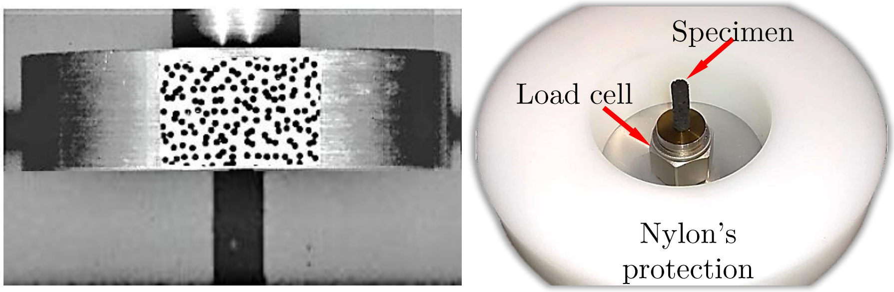

Figure 7: Specimen over load cell (left) and hammer over the specimen (right).

Obviously, its numerical implementation does not offer any geometric difficulty. As it has been stated, for impact test simulation LS-DYNA® software has been selected. The calculations are made by the explicit method. For symmetry reasons, a quarter of the geometry has been modeled as it can be see in Figure 8. Although the problem posses axial symmetry, no 2D modelization was possible because it is not implemented for BB material model.

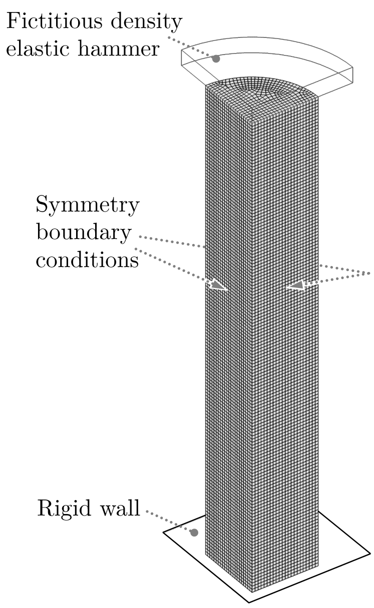

Figure 8: One-quarter pellet-hammer-rigid plane model.

Figure 8 shows, the cylinder (BB material) stays over a rigid surface playing the role of the load cell, i.e., the reaction over this rigid surface can be compared with the results obtained from the load cell during the tests. The hammer is defined by another cylindrical body with aluminum elastic properties and a fictitious value of density in order to reproduce the total falling mass.

For all contacts, sliding hypothesis have been considered. The computation starts just in the contact moment, therefore the nominal impact velocities considered, i.e. 2, 4 and 6 m/s (minimum, medium and maximum test velocities in [1]) are established as initial conditions. The nominal dimensions of the rubber cylinder are 4.2 mm of diameter and 15 mm long.

4.1 Convergence analysis

The problem is strongly non linear because contact, non-linear material, high impact velocities and large strains are under consideration.

The necessary convergence analysis must take into account spacial ($\Delta \mathrm{L}$) and temporal (Δt) discretizations. At any event, it must be considered that LS-DYNA® assumes (Δt) as initial time step and changes it as needed.

For this purpose, we have compared the results obtained with three different models. The considered models were defined as:

- Model A: $\Delta \mathrm{L} = 0.5$ mm, $\Delta t = 0.01$ ms.
- Model B: $\Delta \mathrm{L} = 0.2$ mm, $\Delta t = 0.01$ ms.
- Model C: $\Delta \mathrm{L} = 0.2$ mm, $\Delta t = 0.001$ ms.

For this analysis the same material constants set has been considered to avoid the influence of these parameters over the convergence conclusions.

Figure 9 shows that the engineering stress vs. engineering strain results are, essentially, the same for all the analyzed models. In such a situation, we must conclude that the model is stable enough regarding spacial and temporal discretization. Although computational time is not a strong limitation, since the computation time is kept in the order of minutes, model A is about 50 times faster than B or C. For all the indicates considerations, the model A has been fixed for the rest of the computations of the work.

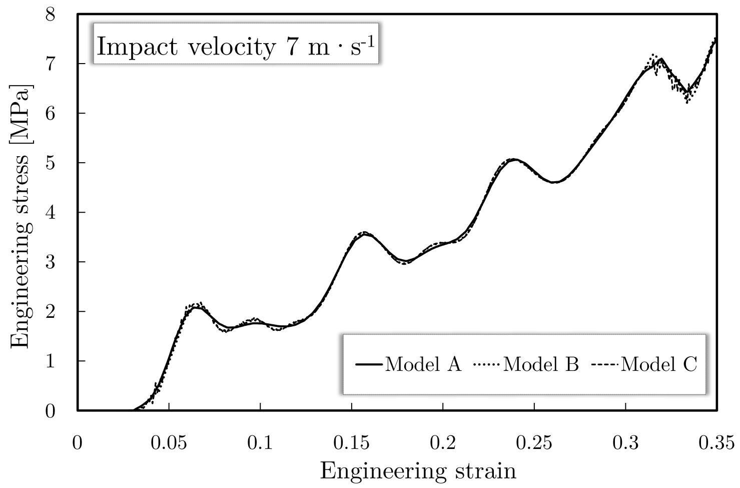

Figure 9: Convergence analysis regarding time and spacial discretizations.

4.2 Numerical results

Figures 10 to 13 show the numerical results obtained (together the experimental results, in grey color) for uncoated and coated pellets, for the two BB formulations investigated. To show the influence of the calibration method, the plots have been grouped according to the calibration algorithm.

As it can be seen, an excellent fit has been obtained for all LS-sets and for all strain rates (Figures 10 to 12). These results show that all the calibration procedures have led to parameter sets that faithfully reproduce the behavior of the material, regardless the objective function and/or optimization algorithm used. As indicated above, this suggests that the separate consideration of the behavior parameters, for comparison purposes, for instance, makes not sense. They must be considered as part of a whole. This "whole" is a closed group of parameters that bring us to a specific viscoelastic material behavior.

On the contrary, the PUM-sets (Figure 13) have shown, for a strain rate of 400 s^{-1}, much more rigid results than the experimental ones, except for the GSM algorithm whose results are good enough. In such a scenario, we have decide do not use PUM-sets for the rest of velocities considering the dispersion of the results for that strain rate.

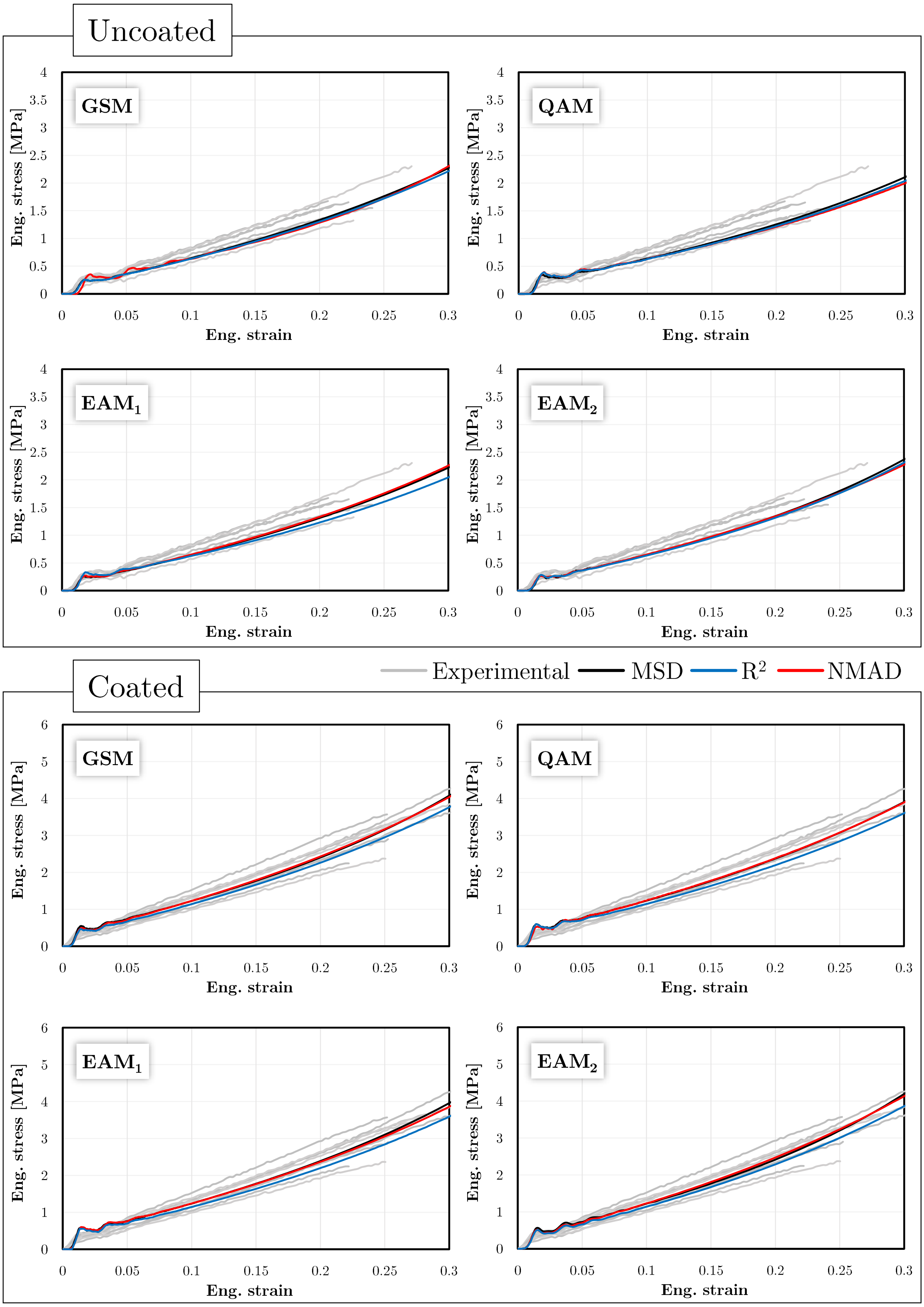

Figure 10: Numerical results, via LS-DYNA® native solver, for coated and uncoated LS-sets, considering a strain rate of $133.33\ s^{-1}$.

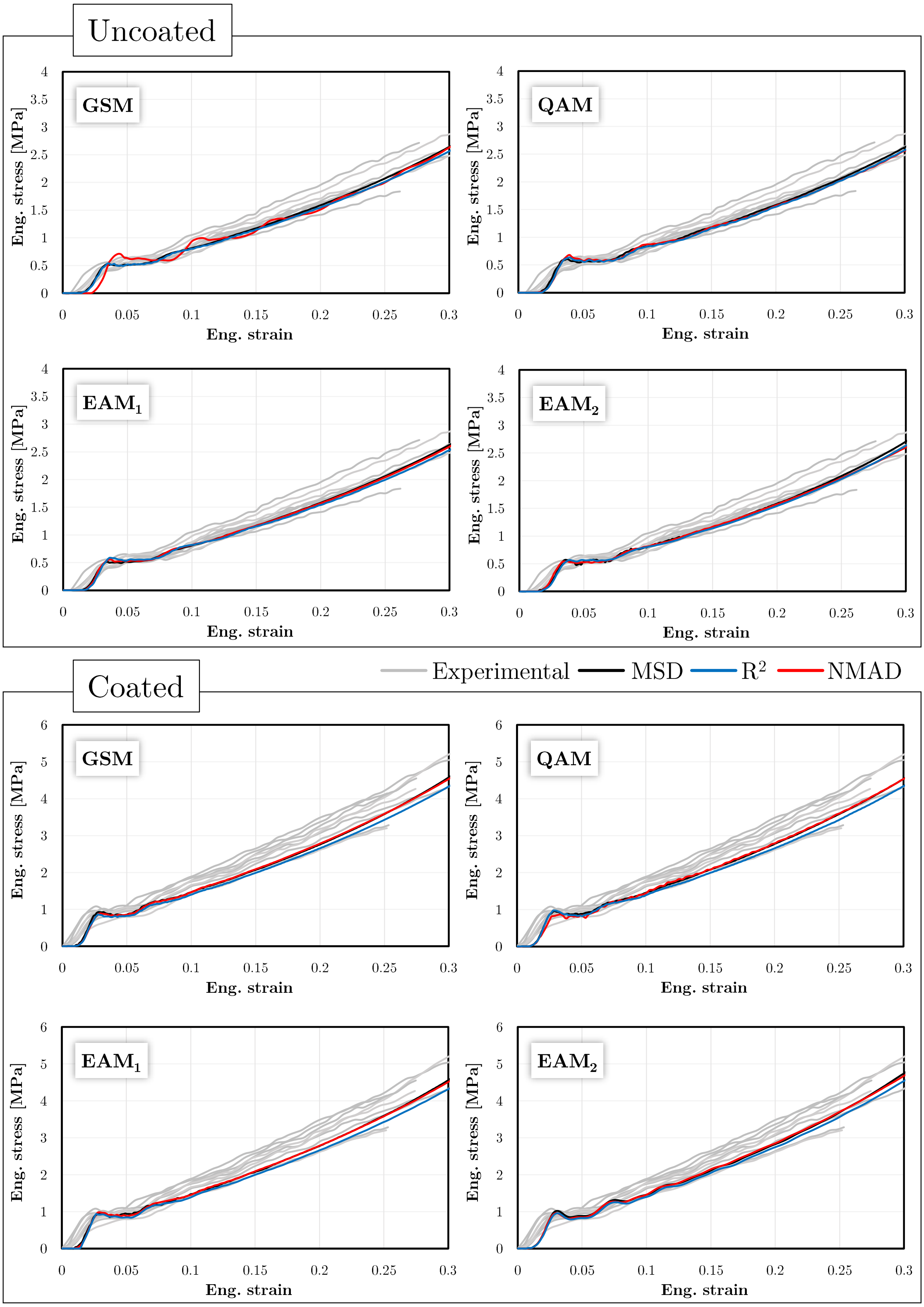

Figure 11: Numerical results, via LS-DYNA® native solver, for coated and uncoated LS-sets, considering a strain rate of $266.66\ s^{-1}$.

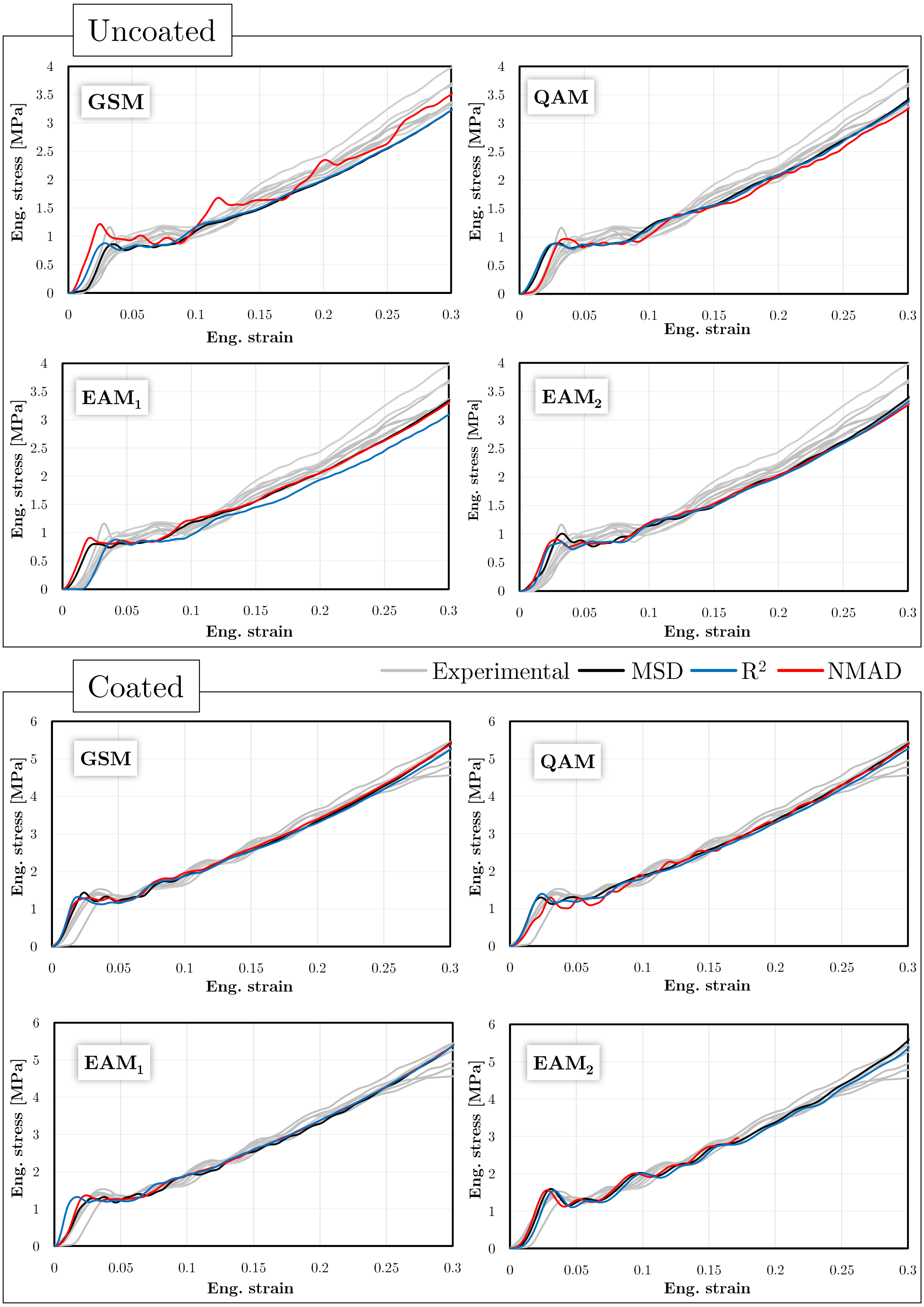

Figure 12: Numerical results, via LS-DYNA® native solver, for coated and uncoated LS-sets, considering a strain rate of $400\ s^{-1}$.

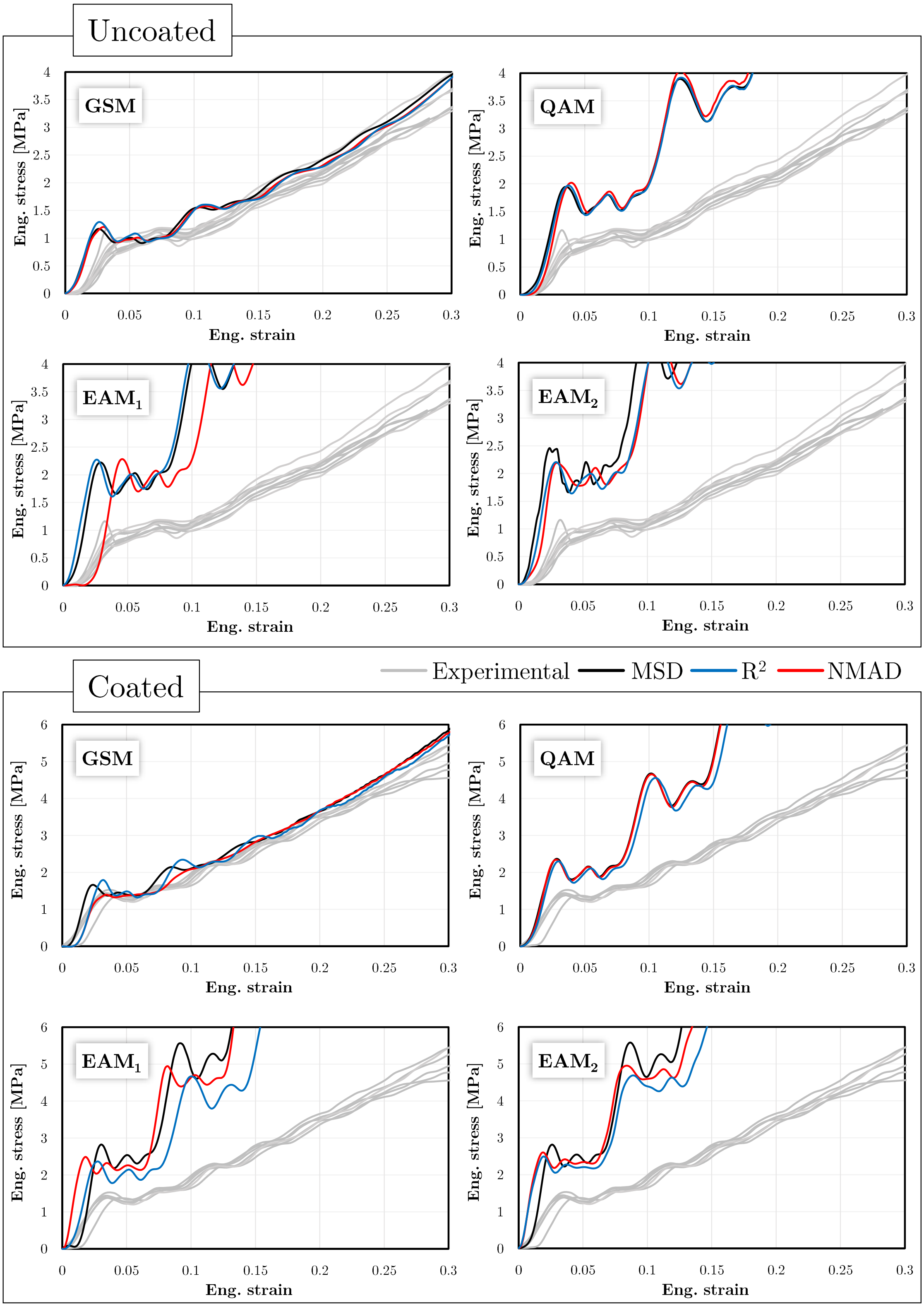

Figure 13: Numerical results, via PolyUmod® solver, for coated and uncoated PUM-sets, considering a strain rate of $400\ s^{-1}$.

5 Conclusions

The sets (forty-eight in total) of material parameters, defining a viscoelastic Bergström-Boyce behavior model for a renewed rubber from end of life tires, obtained in [1] by mean of an experimental procedure, have been compared from a numerical point of view.

To this aim, the software LS-DYNA® has been used to simulate compression impact tests applying impact velocities of 2, 4 and $6\ m/s$; that means strain rates of 133.33, 266.66, and $400\ s^{-1}$, respectively.

Two different solvers have been tested with this software using slightly different approaches of the Bergström-Boyce model: (i) the native LS-DYNA® solver based on the work published in 2009 by Dal and Kaliske [17] and the solver developed by PolymerFEM® called PolyUmod®, [19], based on Bergström formulation [21].

Our results indicate that, using the native solver of LS-DYNA®, all the material parameters sets give us material behaviors fitting perfectly with experimental results for all considered strain rates. On the contrary, more rigid material behaviors are found using the PolyUmod® solver by PolymerFEM®, except for GSM optimization algorithm that give, as well, a material behavior fitting well enough whit our experimental findings.

In summary, in a frame where a strong limiting shape of specimens does not allow to make more than one kind of test, we have demonstrated that the compression impact test, followed an optimization procedure (for instance, the ones include in MCalibration® software), can give us very good results to obtain the nine parameters necessary to define the BB viscoelastic model of a renewed recycled. That is, a useful tool has been developed to facilitate the implementation of this kind of materials in a finite element code for further numerical computations.

6 Acknowledgments

The authors want to show their gratefully to:

- Consejería de Economía y Conocimiento of Junta de Andalucía and the European Regional Development Fund through the project UMA20-FEDERJA-028 for its financial support.
- Spanish Ministry of Financial and Competitiveness for the funds granted by mean of the projects with refs. UNMA13-1E-1901 and UNMA15-CE-3571. These grants allowed to acquire the experimental equipment used in this work.

References

[1] Joaquín González-Vega, Germán Castillo-López, Juan M. Galindo-Moreno, Sergio Guerrero-Porras, and Felipe García-Sánchez. Experimental viscoelastic properties evaluation, under impact loads and large strain conditions, of coated & uncoated rubber from end-of-life tires. *Polymer Testing*, 107:107468, 2022.

[2] Lei Pan, Hong Hao, Jian Cui, and Thong M. Pham. Numerical study on dynamic properties of rubberised concrete with different rubber contents. *Defence Technology*, 2022.

[3] Xin Gao, Wei Guo, Yuxiao Ren, and Wenqian Zeng. Numerical analysis of a double layer rubber dam. *Geotextiles and Geomembranes*, 50(2):249–261, 2022.

[4] Prateek Kumar Dhir, Enrico Tubaldi, Hamid Ahmadi, and Julia Gough. Numerical modelling of reinforced concrete frames with masonry infills and rubber joints. *Engineering Structures*, 246(June):112833, 2021.

[5] Yang Yang, Xingyi Zhu, Denis Jelagin, Alvaro Guarin, and Wynand JvdM Steyn. Numerical analysis concerning the skid resistance of rubber-contaminated runway grooves. *Tribology International*, 163(March):107157, 2021.

[6] D. X. Leng, C. Huang, K. Xu, Y. Ma, G. J. Liu, and Z. X. Li. Experimental mechanics and numerical prediction on stress relaxation and unrecoverable damage characteristics of rubber materials. *Polymer Testing*, 98(March), 2021.

[7] Chen Liu, Bochao Gu, Jianfeng Chen, Liqun Zhang, Yonglai Lu, and Fanzhu Li. Thermo-mechanical coupling analysis of edge-cracked rubber specimen focusing on the crack tip: Experimental observation and numerical simulation. *Materials Today Communications*, 31(March):103348, 2022.

[8] Bin Zhuo, Muyuan Zhu, Yong Fang, Feiyang Wang, Yuxiang Yao, and Sheng Li. Numerical and experimental analyses for rubber-sand particle mixtures applied in high-filled cut-and-cover tunnels. *Construction and Building Materials*, 306(April):124874, 2021.

[9] P. Šulc, J. Kopačka, L. Pešek, and V. Bula. Hyperelastic proportional damping for numerical nonconservative dynamic models of hard rubbers under large deformations. *International Journal of Non-Linear Mechanics*, 137(February):103823, 2021.

[10] Xuan Dai Nguyen and Lotfi Guizani. Analytical and numerical investigation of natural rubber bearings incorporating U-shaped dampers behaviour for seismic isolation. *Engineering Structures*, 243(May):112647, 2021.

[11] Javad Sheikhi, Mojtaba Fathi, Rohola Rahnavard, and Rebecca Napolitano. Numerical analysis of natural rubber bearing equipped with steel and shape memory alloys dampers. *Structures*, 32(March):1839–1855, 2021.

[12] Ahmad Modhej and Seyed Mehdi Zahrai. Numerical study of visco-hyperelastic damper with high axial damping rubber subjected to harmonic loading. *Structures*, 29(October 2020):1550–1561, 2021.

[13] Afshin Anssari-Benam and Cornelius O. Horgan. A three-parameter structurally motivated robust constitutive model for isotropic incompressible unfilled and filled rubber-like materials. *European Journal of Mechanics - A/Solids*, page 104605, 2022.

[14] J. S. Bergström and M. C. Boyce. Constitutive modeling of the large strain time-dependent behavior of elastomers. *Journal of the Mechanics and Physics of Solids*, 1998.

[15] Jörgen Bergström. *Mechanics of Solid Polymers: Theory and Computational Modeling*. 2015.

[16] Ellen M. Arruda and Mary C. Boyce. A three-dimensional constitutive model for the large stretch behavior of rubber elastic materials. *Journal of the Mechanics and Physics of Solids*, 41(2):389–412, 1993.

[17] Hüsnü Dal and Michael Kaliske. Bergström–Boyce model for nonlinear finite rubber viscoelasticity: theoretical aspects and algorithmic treatment for the FE method. *Computational Mechanics*, 44(6):809–823, nov 2009.

[18] J. S. Bergström and M. C. Boyce. Large strain time-dependent behavior of filled elastomers. *Mechanics of Materials*, 2000.

[19] PolymerFEM LLC. PolyUMod_Manual.

[20] Nathan. LS-DYNA ® KEYWORD USER'S MANUAL VOLUME II Material Models LIVERMORE SOFTWARE TECHNOLOGY (LST), AN ANSYS COMPANY. Technical report, 1992.

[21] Jörgen Bergström. *Mechanics of Solid Polymers: Theory and Computational Modeling*. 2015.

Appendix: Sets of material properties

Table 3: Uncoated rubber Bergström-Boyce material parameters computed with MCalibration® with different objective functions and optimization algorithms. PUM-set.

Objective function: R^2				
Mat. param.	GSM	EAM_1	EAM_2	QAM
$\mu[MPa]$	1.34026	1.33085	1.34837	0.988256
$\lambda_L[-]^*$	1.92601	4.83104	1.01194	4.19013
$\kappa[MPa]$	94.3357	247.874	25.1271	53.9454
$s[-]$	4.49308	4.48519	4.70662	4.75959
$\xi[-]$	0.0920818	0.0763386	0.0600704	0.0342387
$C[-]$	-1.20265	-1.19497	-1.2326	-1.41137
$\tau_{base}[MPa]$	0.0237422	0.0287715	0.0413614	0.205705
$m[-]$	1.10006	1.1	1.10004	1.29891
$\hat{\tau}_{cut}[-]$	0.131032	3.64526E-05	5.75453E-04	2.79737E-06
Objective function: MSD				
$\mu[MPa]$	1.29644	1.34931	1.28744	0.842169
$\lambda_L[-]$	4.61006	5.51679	5.3315	4.07178
$\kappa[MPa]$	90.5243	39.2058	509.452	208.867
$s[-]$	5.50858	4.65477	5.44264	5.58939
$\xi[-]$	3.68858E-03	0.0814253	0.00416792	0.0277595
$C[-]$	-0.244413	-1.29467	-0.256971	-1.3052
$\tau_{base}[MPa]$	5.90185E-03	0.0362179	6.14563E-03	0.227438
$m[-]$	1.10008	1.10005	1.10002	1.30008
$\hat{\tau}_{cut}[-]$	0.0729218	1.03411E-05	2.31427E-04	1.35529E-04
Objective function: $NMAD$				
$\mu[MPa]$	1.46354	1.41855	1.43208	0.991328
$\lambda_L[-]$	4.573	8.87012	9.99999	4.026
$\kappa[MPa]$	107.231	65.7427	776.712	72.2666
$s[-]$	4.38364	4.53356	4.36757	5.10904
$\xi[-]$	0.181987	0.0797648	0.0959663	0.0232835
$C[-]$	-1.9999	-1.14582	-1.27254	-1.25543
$\tau_{base}[MPa]$	0.0368353	0.0239409	0.025414	0.207243
$m[-]$	1.10001	1.10003	1.1	1.40888
$\hat{\tau}_{cut}[-]$	0.0677903	1.59102E-06	1.05561E-05	2.1036E-06

* Note: $[-]$ stands for non-dimensional parameters.

Table 4: Coated rubber Bergström-Boyce material parameters computed with MCalibration® with different objective functions and optimization algorithms. PUM-set.

Objective function: R^2				
Mat. param.	GSM	EAM_1	EAM_2	QAM
$\mu[MPa]$	2.50012	1.88608	2.45376	1.63457
$\lambda_L[-]^*$	7.75021	9.02668	9.9449	3.86084
$\kappa[MPa]$	131.646	36.3555	4.01978	82.7037
$s[-]$	4.04338	3.67438	7.09626	3.92806
$\xi[-]$	0.501883	0.0546378	0.0668903	0.0350974
$C[-]$	-1.85078	-1.34949	-1.37323	-1.23014
$\tau_{base}[MPa]$	9.04048E-03	0.199065	0.122597	0.267285
$m[-]$	1.10045	1.35179	1.10007	1.39733
$\hat{\tau}_{cut}[-]$	0.411756	1.18929E-03	1.74477E-04	2.37506E-05
Objective function: MSD				
$\mu[MPa]$	2.65241	2.53468	2.55551	1.87502
$\lambda_L[-]$	4.28802	4.61829	4.20695	4.32939
$\kappa[MPa]$	134.192	60.012	37.306	126.352
$s[-]$	4.33337	4.12229	4.24537	3.53975
$\xi[-]$	0.370754	0.182054	0.134754	0.0328437
$C[-]$	-1.99233	-1.71322	-1.28738	-1.23724
$\tau_{base}[MPa]$	0.0262923	0.0710039	0.0550753	0.311347
$m[-]$	1.27305	1.37776	1.37169	1.65195
$\hat{\tau}_{cut}[-]$	0.0539014	2.0077E-05	1.49938E-04	7.68007E-05
Objective function: $NMAD$				
$\mu[MPa]$	0.744569	2.58127	2.92152	1.91472
$\lambda_L[-]$	2.84639	5.49782	8.21188	4.4038
$\kappa[MPa]$	119.386	8.23856	4.59175	69.6776
$s[-]$	15.7522	4.16538	6.48776	3.44977
$\xi[-]$	2.05457E-04	0.0761447	0.169006	0.0327584
$C[-]$	-0.598766	-1.00045	-1.65287	-1.23422
$\tau_{base}[MPa]$	0.426534	0.0607868	0.0589643	0.29799
$m[-]$	2.40358	1.33118	1.15687	1.58273
$\hat{\tau}_{cut}[-]$	0.0994694	5.03988E-03	6.42446E-04	1.91128E-04

* Note: $[-]$ stands for non-dimensional parameters.

Table 5: Uncoated rubber Bergström-Boyce material parameters computed with MCalibration® with different objective functions and optimization algorithms. LS-set.

Objective function: R^2				
Mat. param.	GSM	EAM$_1$	EAM$_2$	QAM
$K[MPa]$	75.3252	50.2622	18395.4	33.8796
$G[MPa]$	1.36968	0.830381	0.901717	0.37085
$G_v[MPa]$	6.36656	5.77585	6.53338	6.32382
$N[-]$	99.6772	41.7063	2.29564	32.0326
$N_v[-]$	5.82771	40.61097	79.7834	11.1938
$C[-]$	-0.119951	-0.349144	-0.0743961	-0.583433
$m[-]$	1.00093	1.42552	1	1.80915
$\dot{\gamma}_0[-]$	20.758	2.9047	8.35248	4.72051
$\hat{\tau}[MPa]$	0.0197794	0.0385755	6.09509E-03	0.220961
Objective function: MSD				
$K[MPa]$	55.3996	30.2588	321.118	60.4707
$G[MPa]$	1.36805	1.28599	0.903094	0.603831
$G_v[MPa]$	7.6038	8.58727	6.48174	6.96006
$N[-]$	27.3967	49.702	2.24096	3.27879
$N_v[-]$	11.4782	24.6548	7.22054	26.3723
$C[-]$	-0.139658	-0.196904	-0.0854983	-0.374299
$m[-]$	1.00013	1.09283	1	1.47036
$\dot{\gamma}_0[-]$	18.6164	8.65338	10.4818	9.39844
$\hat{\tau}[MPa]$	0.0202637	0.0179877	8.41019E-03	0.10826
Objective function: $NMAD$				
$K[MPa]$	11.7217	18.9677	35.0249	36.4951
$G[MPa]$	0.549087	1.34017	1.40203	0.44048
$G_v[MPa]$	4.88889	5.87115	7.68604	5.86648
$N[-]$	1.53171	10.2626	20.4978	30.4479
$N_v[-]$	36.2132	2.55421	72.0867	8.03569
$C[-]$	-0.0364618	-0.109287	-0.0987081	-0.468072
$m[-]$	1.06323	1.0148	1.00017	1.62321
$\dot{\gamma}_0[-]$	0.015764	5.07883	15.4136	12.7232
$\hat{\tau}[MPa]$	2.48294E-05	5.15362E03	0.0132344	0.257869

* Note: $[-]$ stands for non-dimensional parameters.

Table 6: Coated rubber Bergström-Boyce material parameters computed with MCalibration® with different objective functions and optimization algorithms. LS-set.

Objective function: R^2				
Mat. param.	GSM	EAM_1	EAM_2	QAM
$K[MPa]$	328.413	17.0485	5.31727	236.556
$G[MPa]$	2.11136	1.16024	1.57776	0.97714
$G_v[MPa]$	11.8199	13.4354	54.7574	11.4656
$N[-]$	96.297	30.9275	2.59054	18.4212
$N_v[-]$	60.8691	5.21101	3.92578	23.8223
$C[-]$	-0.191671	-0.531035	-0.239122	-0.583079
$m[-]$	1.3714	1.9676	1.29698	2.08131
$\dot{\gamma}_0[-]$	12.3107	7.64456	2.88066	7.06041
$\hat{\tau}[MPa]$	0.0669289	0.373249	0.036286	0.423624
Objective function: MSD				
$K[MPa]$	338.955	456.348	325.852	241.335
$G[MPa]$	1.41681	1.11708	2.82972	1.13497
$G_v[MPa]$	2.54682	11.8316	3.68733	11.4977
$N[-]$	2.32533	2.87274	10	3.72245
$N_v[-]$	1.18414	38.7349	20	23.7965
$C[-]$	-0.208093	-0.523564	-0.511914	-0.554162
$m[-]$	1.67213	2.2063	1.46382	2.22208
$\dot{\gamma}_0[-]$	2.0815	5.48824	2.36708	6.40869
$\hat{\tau}[MPa]$	0.0360323	0.287584	0.883848	0.351342
Objective function: $NMAD$				
$K[MPa]$	274.035	61.8058	5.80623	660.283
$G[MPa]$	2.35532	1.25398	2.73049	1.43318
$G_v[MPa]$	6.81576	11.6262	23.4285	10.7083
$N[-]$	81.7096	18.5157	36.566	19.5279
$N_v[-]$	2.06109	66.2235	1.43404	21.8841
$C[-]$	-0.167303	-0.585904	-0.170572	-0.510513
$m[-]$	1.47819	2.24973	1.33132	2.12298
$\dot{\gamma}_0[-]$	5.67494	6.51861	10.6935	5.53933
$\hat{\tau}[MPa]$	0.0402549	0.419979	0.0696675	0.286379

* Note: $[-]$ stands for non-dimensional parameters.